International Journal of Nanomedicine

Dovepress

open access to scientific and medical research

Open Access Full Text Article

ORIGINAL RESEARCH

Long-Term Accumulation, Biological Effects and Toxicity of BSA-Coated Gold Nanoparticles in the Mouse Liver, Spleen, and Kidneys

Kristina Jakic[1], Michal Selc[1,2], Filip Razga[3], Veronika Nemethova[3], Petra Mazancova[3], Filip Havel[4,5], Michal Sramek[5], Monika Zarska[5], Jan Proska[4], Vlasta Masanova[6], Iveta Uhnakova[6], Peter Makovicky[7], Marta Novotova[8], Vit Vykoukal[9], Andrea Babelova[1,2]

[1]Department of Nanobiology, Cancer Research Institute, Biomedical Research Center, Slovak Academy of Sciences, Bratislava, Slovakia; [2]Centre for Advanced Material Application, Slovak Academy of Sciences, Bratislava, Slovakia; [3]Selecta Biotech SE, Bratislava, Slovakia; [4]Department of Physical Electronics, Faculty of Nuclear Sciences and Physical Engineering, Czech Technical University in Prague, Prague, Czech Republic; [5]Department of Genome Integrity, Institute of Molecular Genetics of the Czech Academy of Sciences, Prague, Czech Republic; [6]Department of Metallomics, Faculty of Medicine, Slovak Medical University, Bratislava, Slovakia; [7]Department of Molecular Oncology, Cancer Research Institute, Biomedical Research Center, Slovak Academy of Sciences, Bratislava, Slovakia; [8]Department of Cellular Cardiology, Institute of Experimental Endocrinology, Biomedical Research Center, Slovak Academy of Sciences, Bratislava, Slovakia; [9]Department of Chemistry, Faculty of Science, Masaryk University, Brno, Czech Republic

Correspondence: Andrea Babelova, Department of Nanobiology, Cancer Research Institute, Biomedical Research Center, Slovak Academy of Sciences, Bratislava, Slovakia, Tel +421-2-32295-189, Fax +421-2-5477-4284, Email andrea.babelova@savba.sk

Introduction: Gold nanoparticles are promising candidates as vehicles for drug delivery systems and could be developed into effective anticancer treatments. However, concerns about their safety need to be identified, addressed, and satisfactorily answered. Although gold nanoparticles are considered biocompatible and nontoxic, most of the toxicology evidence originates from in vitro studies, which may not reflect the responses in complex living organisms.

Methods: We used an animal model to study the long-term effects of 20 nm spherical AuNPs coated with bovine serum albumin. Mice received a 1 mg/kg single intravenous dose of nanoparticles, and the biodistribution and accumulation, as well as the organ changes caused by the nanoparticles, were characterized in the liver, spleen, and kidneys during 120 days.

Results: The amount of nanoparticles in the organs remained high at 120 days compared with day 1, showing a 39% reduction in the liver, a 53% increase in the spleen, and a 150% increase in the kidneys. The biological effects of chronic nanoparticle exposure were associated with early inflammatory and fibrotic responses in the organs and were more pronounced in the kidneys, despite a negligible amount of nanoparticles found in renal tissues.

Conclusion: Our data suggest, that although AuNPs belong to the safest nanomaterial platforms nowadays, due to their slow tissue elimination leading to long-term accumulation in the biological systems, they may induce toxic responses in the vital organs, and so understanding of their long-term biological impact is important to consider their potential therapeutic applications.

Keywords: AuNPs, in vivo, long-term accumulation, biodistribution, inflammation, fibrosis

Introduction

The development of novel, highly selective, tissue-specific, nano-based agents for specific diagnostic and therapeutic purposes is the objective of modern nanomedicine. Gold nanoparticles appear to be an ideal tool for reaching this goal because of their unique physical and chemical properties. The use of gold in medicine is not new. This valuable noble metal has been used in the treatment of various diseases[1] for centuries, such as for rheumatoid arthritis.[2] Gold nanoparticles (AuNPs) are considered biocompatible and possess remarkable optical, photonic, and electronic properties, which makes them suitable for use in diagnostics, imaging, and various therapeutic applications.[3–5] Some AuNP-based formulations have been tested in clinical trials.[6] Their clinical use, however, remains limited. One reason for this is the lack of information about the long-term effects of AuNPs and thus their safety. The mechanisms involved in nanoparticle

Received: 12 December 2023
Accepted: 18 April 2024
Published: 8 May 2024

Graphical Abstract

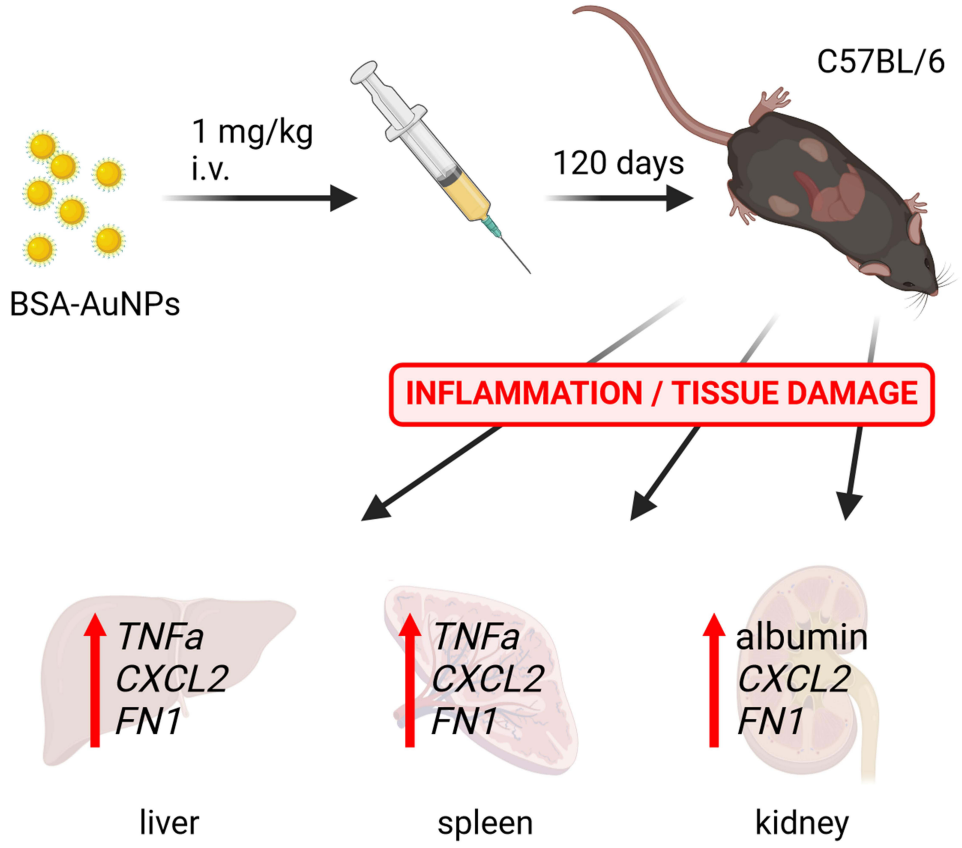

internalization, short-term biodistribution,[7] and acute toxicity[8] have been studied extensively, whereas their long-term impact related to nanoparticle accumulation in organs remains relatively unexplored. The slow tissue clearance of AuNPs may increase their toxicity.[9,10] AuNPs preferably accumulate in the liver and spleen[11] regardless of surface coating.[12] However, it remains unclear whether only these organs would be affected by the long-term accumulation of AuNPs and if other organs with no detectable nanoparticle accumulation would be spared. Therefore, evaluation of the long-term effects of AuNPs is essential to determine their toxicity.[13] This study examined the long-term accumulation, biological effects, and possible elimination of AuNPs after 120 days in a mouse model. Bovine serum albumin-coated AuNPs (BSA-AuNPs, 20 nm) were used because of the low toxicity of BSA functionalization in vivo.[14] The electrostatic interaction-based synthesis of BSA-AuNPs was chosen to reduce the additional toxic effect of additives used in conventional AuNPs conjugation strategies.[15] Considering that intraperitoneal and per oral administration routes are linked to higher toxicity than intravenous application,[16,17] a single intravenous dose of BSA-AuNPs was administered, and C57BL/6 mice were monitored over a period of 4 months focusing on three vital organs: the liver, spleen, and kidneys. The impact of chronic exposure of tissues to BSA-AuNPs was examined by assessing the expression of inflammatory and fibrotic genes at the mRNA and protein levels, histological and immunohistological analyses, and transmission electron microscopy (TEM).

Materials and Methods

Gold Nanoparticles

Gold nanoparticles were prepared by the Turkevich method.[18] Synthesis was finely tuned to achieve 20 nm spherical nanoparticles. The initial concentrations of gold ions and sodium tris-citrate were set to 0.266 mM, and 1.814 mM,

respectively. BSA-AuNPs were prepared by binding BSA to citrate-capped AuNPs.[15] First, the as-synthetized AuNPs were distributed by 8 mL to falcon tubes and purified by centrifugation at 9000 rpm for 25 min. Supernatant was discarded and each falcon tube was enriched by 2.5 mL of 15 mg/mL BSA. Particles were sonicated and kept at 30 °C for 30 min, then stored at RT for one week. After one week, the particles were diluted with milli-Q water to the original volume of 8 mL per falcon tube, sonicated at 30 °C and centrifuged at 9000 rpm for 30 min. The supernatant was again discarded and sedimented BSA-AuNPs from all falcon tubes were redispersed in one 50-mL falcon tube and diluted with milli-Q water to the desired concentration. Finally, the BSA-AuNPs were filtered through a 0.22 μm pore size filter in a sterile environment. The size and shape of the gold core were characterized by JSM-7500F JEOL field emission scanning-electron microscope (FE-SEM; JEOL, Japan).

BSA-AuNPs were characterized in water as well as in 5% glucose and the estimated parameters including particle size distribution, hydrodynamic diameter, and Z-average were determined by dynamic light scattering (DLS) using Zetasizer Nano-ZS (Malvern Instruments, UK). The measurements were performed at 3 min intervals during 1 h and every data point was recorded as the average of at least 15 repetitions. The instrument set-up was done with respect to the physico-chemical characteristics (absorption, refractive index, viscosity, temperature) of the studied colloidal solutions.[19]

Animals

Male C57BL/6 mice (Velaz, Czech Republic) at 10 weeks of age were used for BSA-AuNPs application. The animals were housed in an SPF facility with 12/12 hours day/night cycle and had free access to chow and water. Mice (n = 64) were randomly divided into experimental groups. For nanoparticle application, mice were injected intravenously with 100 μL of BSA-AuNPs suspension in 5% glucose as a single dose of 1 mg/kg body weight, via retroorbital sinus. The control group was injected with 100 μL of 5% glucose. Body weight was monitored each 10 days combined with collection of the urine. After 1-, 30-, 60-, and 120-days, the mice were euthanized with i.p. injection of thiopental, and liver, spleen, kidneys, and blood were extracted for further analyses. Plasma was prepared by centrifugation at 600 x g for 15 min and stored at – 80 °C. All animal handlings were done in accordance with The Slovak Animal Protection Act subject to The European Union legislation on animal welfare EU Directive 2010/63/EU for animal experiments and were approved by The Ethics Committee of Biomedical Research Center of the Slovak Academy of Sciences and The State Veterinary and Food Administration of the Slovak Republic under the approval number 597/18-221/3.

ELISA

Albumin level was determined in mouse spot urine samples by Mouse Albumin ELISA Kit (Bethyl Laboratories, USA) according to the manufacturer's recommendations. ALT level was estimated in mouse plasma samples by Mouse ALT Simple Step ELISA Kit (Abcam, UK) according to the manufacturer's recommendations.

Morphological and Immunohistochemical Studies

Organs were fixed in a 10% formalin solution, dehydrated, processed into paraffin blocks and stored for histological and immunohistochemical analyses. Tissue sections (3 μm) were deparaffinized, rehydrated and stained with hematoxylin and eosin (HE) or periodic acid–Schiff reaction (PAS) for the evaluation of general tissue structure.

For immunohistochemistry, antigen retrieval was performed using Digest All Pepsin (LifeTechnologies, USA), followed by inactivation of endogenous peroxidases. Sections were incubated with primary antibody overnight at 4 °C followed by incubation with secondary antibody conjugated with horseradish peroxidase for 2 h at 37 °C. 3,3'-Diaminobenzidine (Vector® DAB, Vector Laboratories, USA) has been used for chromogen visualization and nuclei were counterstained with hematoxylin. Bright-field images of the sections were acquired with Olympus BX46 microscope with an Olympus U-CMAD3 camera (Olympus, Japan). The list of antibodies used for the study is shown in the Table 1.

qRT-PCR

Total RNA from snap-frozen tissue was isolated using TRI reagent (T9424, Sigma-Aldrich, USA) and RNA concentration was measured by BioDrop μLite+ (Biochrom, UK). After treatment with RNase-free DNase I (Thermo Scientific™, USA), 1 μg of RNA was used for transcription into cDNA using Revert Aid First Strand cDNA Synthesis Kit (Thermo

Table 1 List of Antibodies Used for the Study

Antibody	Catalog Nr.	Company
F4/80 (D2S9R) XP® Rabbit mAb	70076	CellSignaling
Anti-Fibronectin antibody produced in rabbit	F3648	Sigma-Aldrich
Anti-rabbit IgG, HRP-linked Antibody	F7074	CellSignaling
Anti-ATP5A antibody	ab245581	Abcam
Anti-ATPB antibody	ab128743	Abcam
Anti-Cytochrome P450 4A/CYP4A11 antibody	ab140635	Abcam

Scientific™, USA). For 20 µL PCR reaction, FastStart Universal SYBR Green Master (ROX) (Roche, Switzerland), 300 nM primers, PCR grade water, and 1 µL cDNA were used. The list of primers used for the study is shown in the Table 2.

PCR was performed using an AriaMx Real-Time PCR instrument (Agilent Technologies, USA) according to the FastStart Universal SYBR Green Master protocol. Relative expression levels of target genes were quantified using the $2^{-\Delta\Delta Ct}$ method. *Polr2a* was used as a housekeeping gene.

Western Blot

The proteins were isolated from the snap-frozen tissues using Cell Lysis Buffer (10X) (Cell Signaling Technology, USA) supplemented with 1 mM PMSF (Cell Signaling Technology, USA) and protein concentration was determined using the Bradford assay. Equal amounts of proteins were boiled in SDS Sample Loading Buffer, separated on 7.5% SDS-PAGE gel, and transferred to a 0.2 µm nitrocellulose membrane (Amersham, UK). After blocking the membrane with 1X ROTI (Carl Roth, Germany) for one hour, the membrane was washed with Tris-buffered saline and Tween 20 (TBS-T) and then incubated at 4 °C overnight with anti-fibronectin antibody (F3648, Sigma-Aldrich, USA). Anti-β-tubulin antibody

Table 2 Primer Sequences Used for the Study

Gene	Primer	Sequence	Length
Tnfa	Forward	5′-CCCACGTCGTAGCAAACCACCAAG-3′	416 bp
	Reverse	5′-TCCAAAGTAGACCTGCCCGGACTC-3′	
Cxcl2	Forward	5′-GCTTCCTCGGGCACTCCAGAC-3′	345 bp
	Reverse	5′-TTAGCCTTGCCTTTGTTCAGTAT-3′	
Xdh	Forward	5′-ATCTGGAGACCCACTGCACC-3′	71 bp
	Reverse	5′-TGTGCTCACGAAGAGCTCCAT-3′	
Col1a1	Forward	5′-GTCCCAACCCCCAAAGAC-3′	78 bp
	Reverse	5′-CATCTTCTGAGTTTGGTGATACGT-3′	
Col3a1	Forward	5′-TGGTTTCTTCTCACCCTTCTTC-3′	73 bp
	Reverse	5′-TGCATCCAAATTCATCTACGT-3′	
Fn1	Forward	5′-ATGCACCGATTGTCAACAGA-3′	428 bp
	Reverse	5′-TGCCGCAACTACTGTGATTC-3′	
Polr2a	Forward	5′-CTCGAAACCAGGATGATCTGACTC-3′	332 bp
	Reverse	5′-CACACCCACTTGGTCAATGGATAG-3′	

(ab6046, Abcam, USA) was used as housekeeping. The next day, the membrane was washed with TBS-T and then incubated with a secondary Goat anti-Rabbit IgG Alexa Fluor™ 680 antibody (A21109, Invitrogen, USA). Proteins were visualized by an Odyssey Imaging System (LI-COR Biosciences, USA) and relative intensities of bands were evaluated using the Image Studio software (LI-COR Biosciences, USA).

Transmission Electron Microscopy (TEM)

Extracted organs were pre-fixed with 2% glutaraldehyde in cacodylate buffer (in mM: 150 Na-cacodylate, 2.0 mM $CaCl_2$; pH 7.3) for 2 hours. Subsequently, small pieces of tissue isolated from the left lobe of liver and spleen were repeatedly fixed with 2% glutaraldehyde in cacodylate buffer for 1 hour, postfixed in cacodylate with 1% osmium tetroxide for 30 min and stained with 1% aqueous uranyl acetate. After dehydration in a graded ethanol series and propylene oxide, the samples were embedded in Durcupan (Fluka, Switzerland). Ultrathin (58–60 nm) sections taken at randomly selected levels of the tissue blocks were cut with a Power-Tome MT-XL (RMC/Sorvall, USA) ultramicrotome, placed on copper grids covered with Formvar and stained with lead citrate. The sections were examined with a JEM 1200 electron microscope (Jeol, Japan). Images were recorded using a Gatan Dual Vision 300W CCD camera (Pleasanton, USA).

Inductively Coupled Plasma Mass Spectroscopy (ICP-MS)

The uptake of BSA-AuNPs by liver, spleen, and kidneys was quantified by ICP-MS. Thawed organ samples were digested with 3.5 mL of 65% HNO_3 and 1.5 mL of 30% H_2O_2 in a high-performance microwave digestion unit (mls 1200 mega, Milestone, Italy). Gold (197Au) concentrations were determined using a quadrupole ICP-MS instrument (XSeries 2, Thermo Scientific™, UK) equipped with a conical nebulizer and a Peltier cooled impact bead spray chamber. Instrumental parameters were standard mode, 1400 W forward power, 30 ms dwell time, flow rates: 0.85 L/min nebulizer gas, 0.70 L/min auxiliary gas, 13 L/min coolant gas, and Ni sample and skimmer cones. Measurements were performed using the calibration curve method with internal standard correction. Terbium solution (10 µg/l in 2% HNO_3) was used as an internal standard. The limit of detection and the limit of quantification of the ICP-MS method were 0.14 µg/l and 0.48 µg/l, respectively.

Statistical Analysis

The data are expressed as a mean value ± standard error from at least three independent experiments. The Shapiro–Wilk and D'Agostino-Pearson tests assessed the distribution of data's normality. For the normal distribution, statistical analyses were performed using Student's *t*-test. For nonparametric distribution, Mann–Whitney test was performed. GraphPad Prism software was used for statistical analyses of the data. Statistical significance among groups: $P < 0.05$ (*), $P < 0.01$ (**), and $P < 0.001$ (***).

Results

The Biodistribution of BSA-AuNPs Does Not Change During the 4-Month Exposure

To investigate the biological impact of BSA-AuNPs on the structure and function of mouse organs during the 4-month exposure, the nanoparticles were characterized before in vivo application. Field emission scanning electron microscopy showed the expected size and shape of the gold core, which was confirmed spectrophotometrically (Figure 1A–C). The colloidal stability of BSA-AuNPs was estimated by dynamic light scattering after their preparation in water as well as in a 5% glucose solution, which was used for in vivo applications (Table 3).

To analyze the long-term distribution of BSA-AuNPs in mouse tissues, a single intravenous injection of 1 mg/kg body weight BSA-AuNPs in 5% glucose was administered to C57BL/6 mice via the retroorbital sinus. The amount of BSA-AuNPs was determined in the liver, spleen, and kidneys at 1, 30, 60, and 120 days after injection. Data from inductively coupled plasma mass spectrometry (ICP-MS) showed that at 24 h after injection, a large amount of BSA-AuNPs had accumulated in the liver, moderate amounts were detected in the spleen, and almost undetectable amounts were found in the kidneys (Figure 2A). Normalization of the amount of gold to organ weight confirmed the higher distribution of BSA-AuNPs in the liver compared with that in the spleen (Figure 2B). The accumulated amounts expressed as a percentage of the applied dose were as follows: 41.41% of the injected BSA-AuNPs accumulated in the liver, 1.28% accumulated in the spleen,

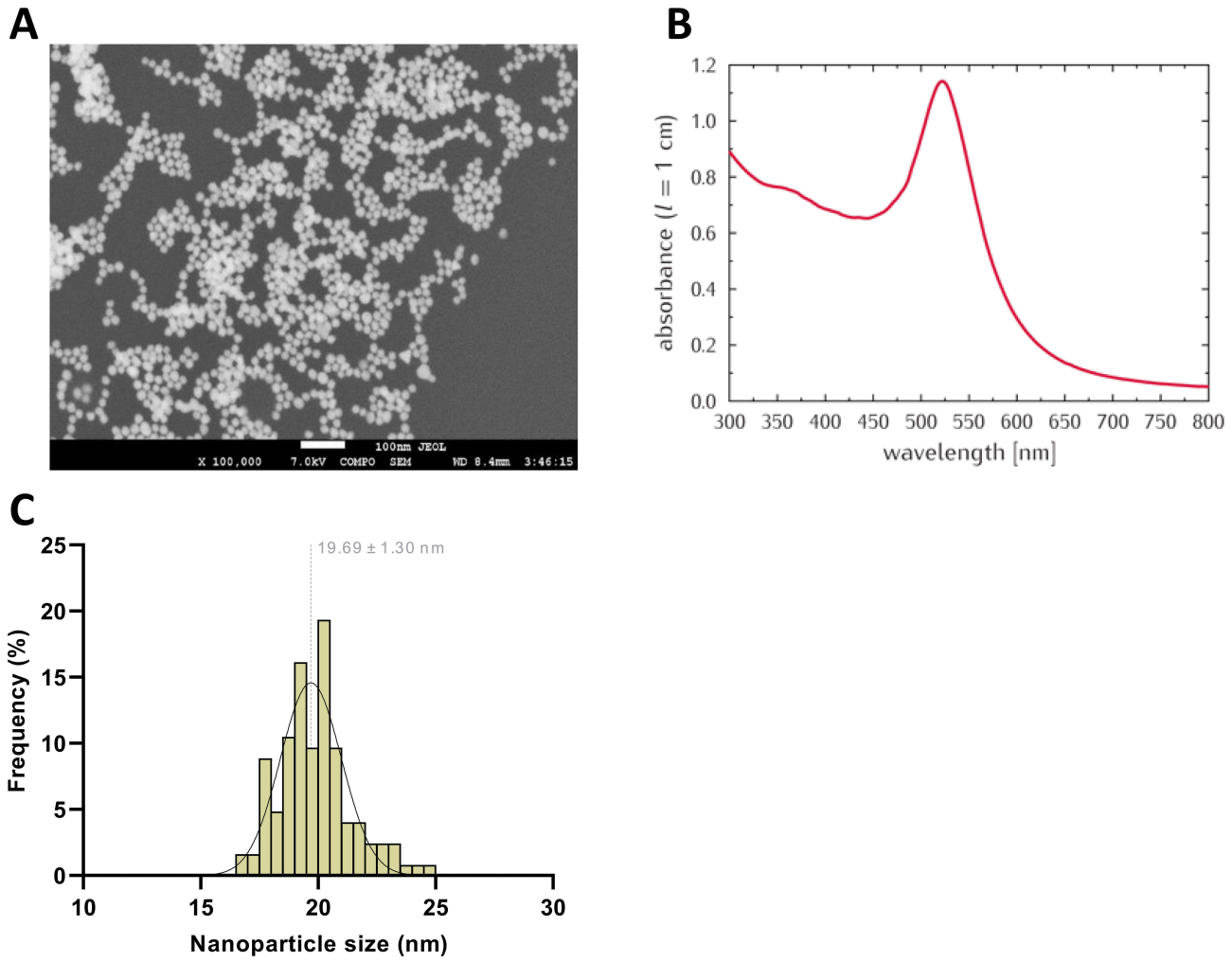

Figure 1 Characterization of BSA-AuNPs after preparation. FE-SEM micrograph of (18.3 ± 1.5 nm) BSA-AuNPs deposited on silicon wafer (**A**). UV-VIS absorption spectrum of BSA-AuNPs (pathlength of 0.4 cm) (**B**). Size distribution of AuNPs in water (**C**).

0.04% accumulated in the kidneys, and 57.27% was not detected in these three organs after 24 h (Figure S1). This distribution pattern changed over 120 days, showing a reduction of accumulated BSA-AuNPs in the liver (25.26%) and an increase in the spleen (1.97%) and kidneys (0.10%) (Figure 2A–D and S1). This resulted in an increase of up to 72.67% in the proportion of BSA-AuNPs that did not accumulate in the organs analyzed (Figure S1). The fate of the BSA-AuNPs that were not detected in the organs analyzed was not investigated; however, it is likely that these nanoparticles, at least in part, were excreted from the mouse body. The elimination of nanoparticles from the liver, spleen, and kidneys over 4 months suggests an ineffective mechanism of clearance of gold nanoparticles from target organs.

Long-Term Exposure to BSA-AuNPs is Associated with Increased Levels of Inflammatory Mediators in the Liver and Spleen

Quantification of BSA-AuNPs in the liver and spleen, which showed high nanoparticle accumulation, revealed that the levels of BSA-AuNPs remained relatively constant over the 120-day period. The levels eventually decreased in the liver,

Table 3 Characteristics of BSA-AuNPs Before Application

Solution	Size Number (nm)	Size Intensity (nm)	Z-Average (nm)	PdI
H_2O	38±5	65±1	45±1	0.261±0.006
5% glucose	48±23	177±35	108±4	0.463±0.017

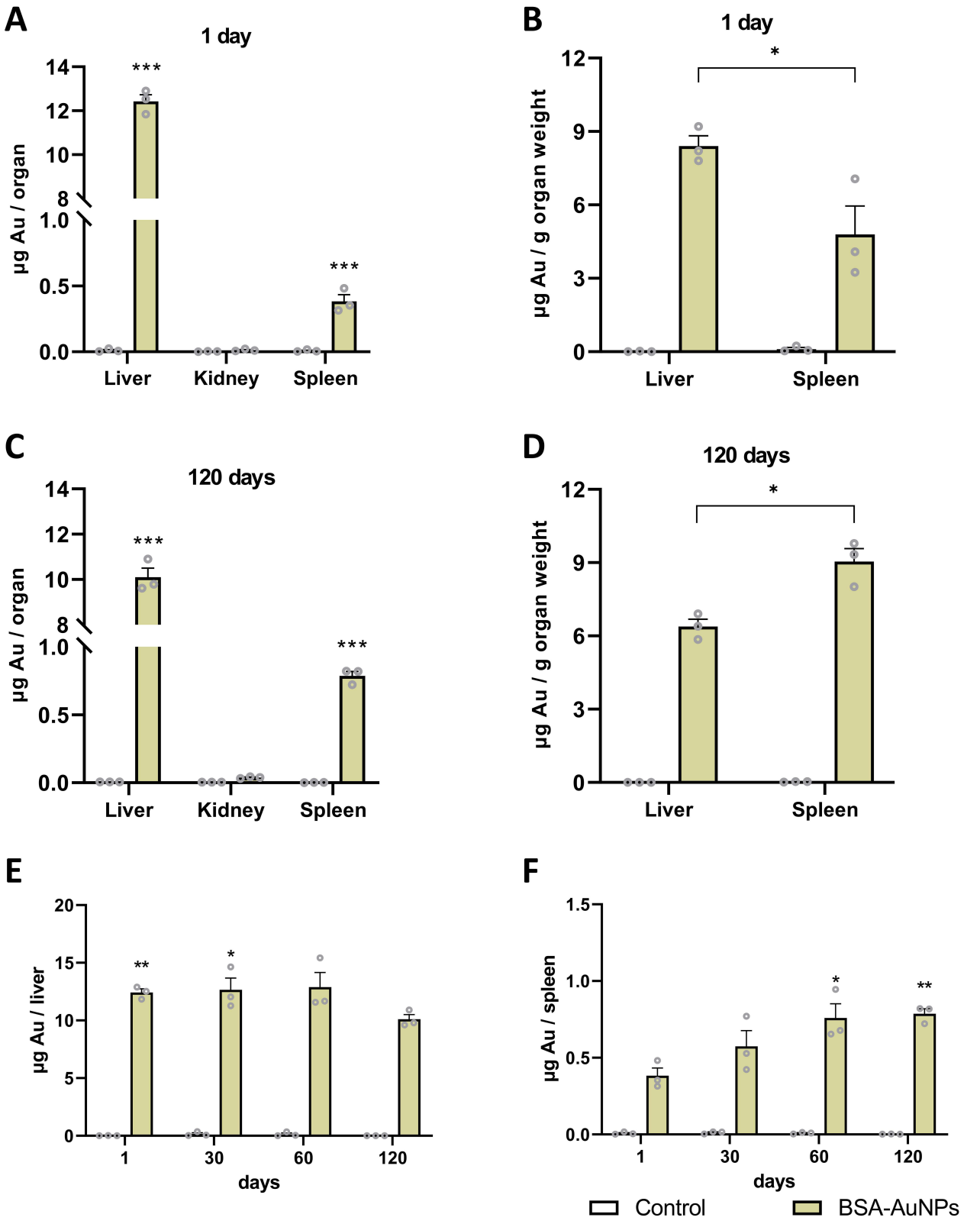

Figure 2 The amount of nanoparticles in mouse liver, kidneys, and spleen after one day (**A**) and the number of nanoparticles per gram of liver and spleen after one day (**B**) after a single application of nanoparticles (asterisks represent statistical differences between untreated and treated groups). The amount of nanoparticles in mouse liver, kidneys, and spleen after 120 days (**C**) and the amount of nanoparticles per gram of liver and spleen after 120 days (**D**) after a single application of nanoparticles (asterisks represent statistical differences between treated groups). The amount of nanoparticles in the liver after 120 days was significantly lower than after 1 and 30 days (**E**), while significantly more nanoparticles accumulated in the spleen after 60 and 120 days than after one day of nanoparticle application (**F**) (asterisks represent statistical differences compared to 120 days (**E**) or 1 day (**F**) treated groups). Data represent the mean ± SEM from three mice. Statistical significance among groups: $P < 0.05$ (*), $P < 0.01$ (**), and $P < 0.001$ (***).

https://doi.org/10.2147/IJN.S443168 DovePress

whereas they increased constantly in the spleen during the course of the experiment (Figure 2E and F). During the first 60 days, the distribution of BSA-AuNPs in the liver changed minimally, that was followed by a gradual decrease at 120 days (Figure 2E). The increase of BSA-AuNPs in the spleen between days 1 and 120 (Figure 2F) suggests that, in addition to the secretion of nanoparticles from organs into the circulation, they could be redistributed among organs. The spleen of mice exposed to BSA-AuNPs for 120 days weighed more than the spleen of control mice (Figure 3A), whereas this was

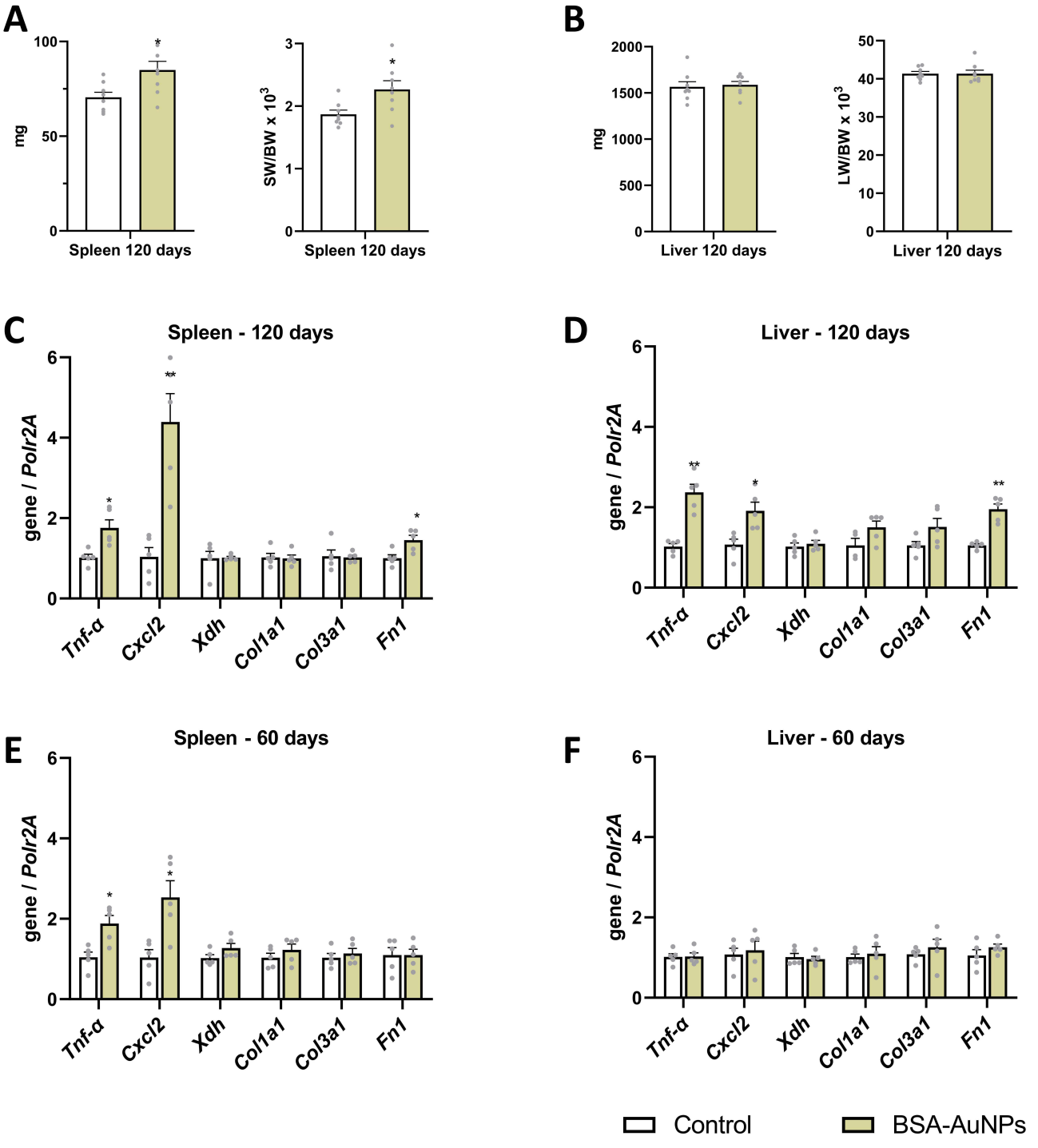

Figure 3 Single administration of nanoparticles resulted in increased spleen weight in the treated mice than in the controls after 120 days of exposure (**A**), while the liver weight of the treated mice did not change compared to the controls (**B**). After 120 days, changes in the expression of some pro-inflammatory genes were observed both in the spleen (**C**) and in the liver (**D**), which were not changed after 60 days, or with less intensity (**E** and **F**). Asterisks represent statistical differences compared to untreated groups. Data from qRT-PCR represent the mean ± SEM of five independent experiments. Statistical significance among groups: $P < 0.05$ (*), $P < 0.01$ (**).

not observed in the liver (Figure 3B). This difference was observed even after normalizing the weight of the spleen to mouse body weight (Figure 3A). In addition to the changes in spleen weight, long-term accumulation of BSA-AuNPs was associated with elevated mRNA levels of *Tnfα, Cxcl2*, and *Fn1* (Figure 3C). Similarly, an increase in *Tnfα, Cxcl2*, and *Fn1* mRNA was observed in the liver after 120 days (Figure 3D) concomitant with BSA-AuNP accumulation. We measured the mRNA levels of these markers at 60 days to determine whether they were activated earlier. At 60 days after injection of BSA-AuNPs, the mRNA levels of *Tnfα* and *Cxcl2* were increased in the spleen (Figure 3E) but not in the liver (Figure 3F). These results suggest that the long-term effects of nanoparticles have a different timeline in different organs in association with their tissue accumulation patterns.

Long-Term Exposure to BSA-AuNPs is Associated with Increased Risk of Fibrosis in the Liver and Spleen

Histological analysis was performed to further examine the long-term effects of BSA-AuNPs on tissue structure. Hematoxylin-eosin staining of the liver showed that the persistence of BSA-AuNPs for 120 days was associated with increased tissue infiltration of mononuclear cells (Figure 4A) that were partially positive for F4/80 (Figure 4B), suggesting an early inflammatory response. The pro-inflammatory activity of these cells together with enhanced fibronectin deposition (Figure 4C) suggests an early pathogenic event related to liver fibrogenesis.[20] Fibronectin deposition and areas of infiltrating cells were not observed in the livers of control mice (Figure 4C). Non-alcoholic fatty liver disease fibrosis scoring confirmed that non-alcoholic steatohepatitis (NASH) parameters were worse in the livers of mice with BSA-AuNPs than in controls after 120 days (Figure S2). These changes did not affect liver function, as indicated by plasma ALT levels (Figure S3). Although the spleens of mice treated with BSA-AuNPs for 120 days were heavier than those of control mice, HE staining showed no structural differences between BSA-AuNP-treated and non-treated mice related to the function of the spleen (Figure 4D). F4/80 staining showed no differences between BSA-AuNPs and untreated controls (Figure 4E). However, the level of fibronectin in the spleen was higher in mice exposed to BSA-AuNPs for 120 days than in the controls (Figure 4F). Consistent with the immunohistochemistry findings, Western blot analysis revealed different amounts of fibronectin in the liver between BSA-AuNPs-treated and untreated mice (Figure 4G). In addition, qRT-PCR detected increase in the proinflammatory mediators *Tnfα* and *Cxcl2* (Figure 3D) was related to F4/80 positivity and increased fibronectin (Figure 4B and C). The results of qRT-PCR (Figure 3C) were consistent with those of Western blotting showing a higher accumulation of fibronectin in the spleens of mice exposed to long-term BSA-AuNPs (Figure 4G). The fact that fibronectin was not increased at earlier time-points, as shown at 60 days (Figure 4H), suggests that the expression of fibronectin is associated with the long-term impact of BSA-AuNPs on tissue remodeling.

BSA-AuNPs Deposit in Phagocytic Cells During the Course of Long-Term Accumulation

The detection of F4/80-positive cells in liver tissues, the infiltration of partially F4/80-positive mononuclear cells in vessels, and increased fibronectin in infiltrates as well as in the blood vessel lining in BSA-AuNP-injected mice suggest a link between these events and the gold nanomaterial content. To investigate this, liver and spleen tissue samples were examined by TEM. Electron-microscopy analysis of liver tissues showed no pathological changes after 120 days of BSA-AuNP exposure. Phagocytic cells were considered to be present more frequently in the sinusoid space of BSA-AuNP-injected mice than in non-injected controls. In line with the immunohistology findings, BSA-AuNPs were detected in endothelial cells (Figure 5A and B) and mainly in phagocytic cells (Figure 5C and D). Nanoparticles were detected as clusters located in the cell cytoplasm (Figure 5B) or accumulated in large phagolysosomes (Figure 5D). No morphological changes were observed in spleen cells. Clusters of gold nanoparticles were detected in supporting and endothelial cells (Figure 6A–D). In macrophages, BSA-AuNPs were detected as clusters and in a dispersed form (Figure 6E and F). These results suggest that immune cells, such as phagocytes, are involved in the transport of BSA-AuNPs from the liver to the spleen and potentially to other organs.

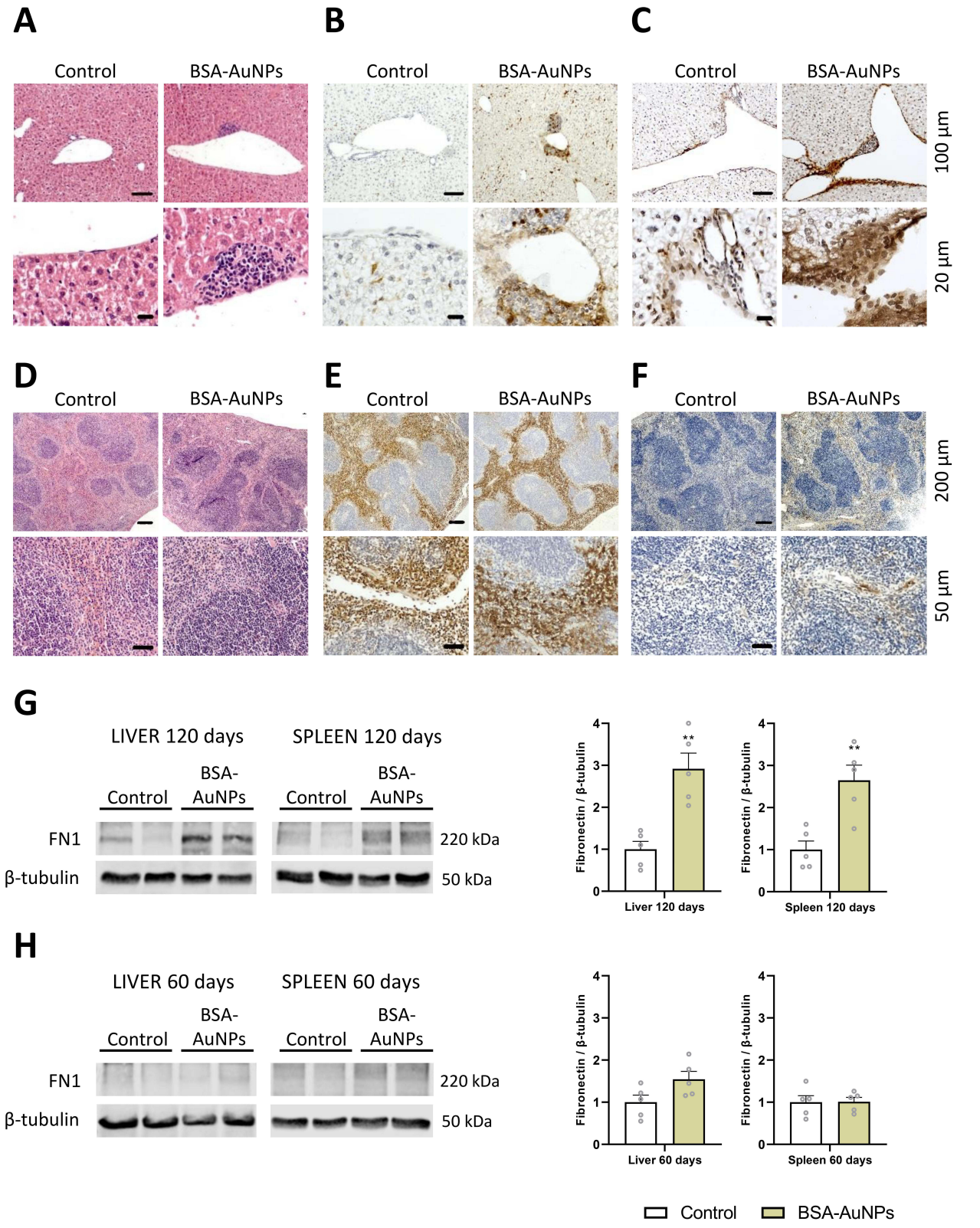

Figure 4 Hematoxylin-eosin staining of liver tissue showed increased infiltration of mononuclear cells (**A**), partial positivity for F4/80 (**B**), and enhanced fibronectin deposition (**C**). Hematoxylin-eosin staining, as well as F4/80 staining of spleen tissue showed any structural disturbances (**D** and **E**), but fibronectin detection revealed higher fibronectin content in spleens exposed to BSA-AuNPs for 120 days (**F**). Differences in fibronectin were also detect between treated and non-treated groups after 120 days by Western blot (**G**), which was not yet observed at 60 days (**H**). Data from Western blot represent the mean ± SEM of five independent experiments. Statistical significance among groups: $P < 0.01$ (**). Magnification (**A**–**C**) upper panel 100x, bar 100 µm, lower panel 400x, bar 20 µm. Magnification (**D**–**F**) upper panel 40x, bar 200 µm, lower panel 200x, bar 50 µm.

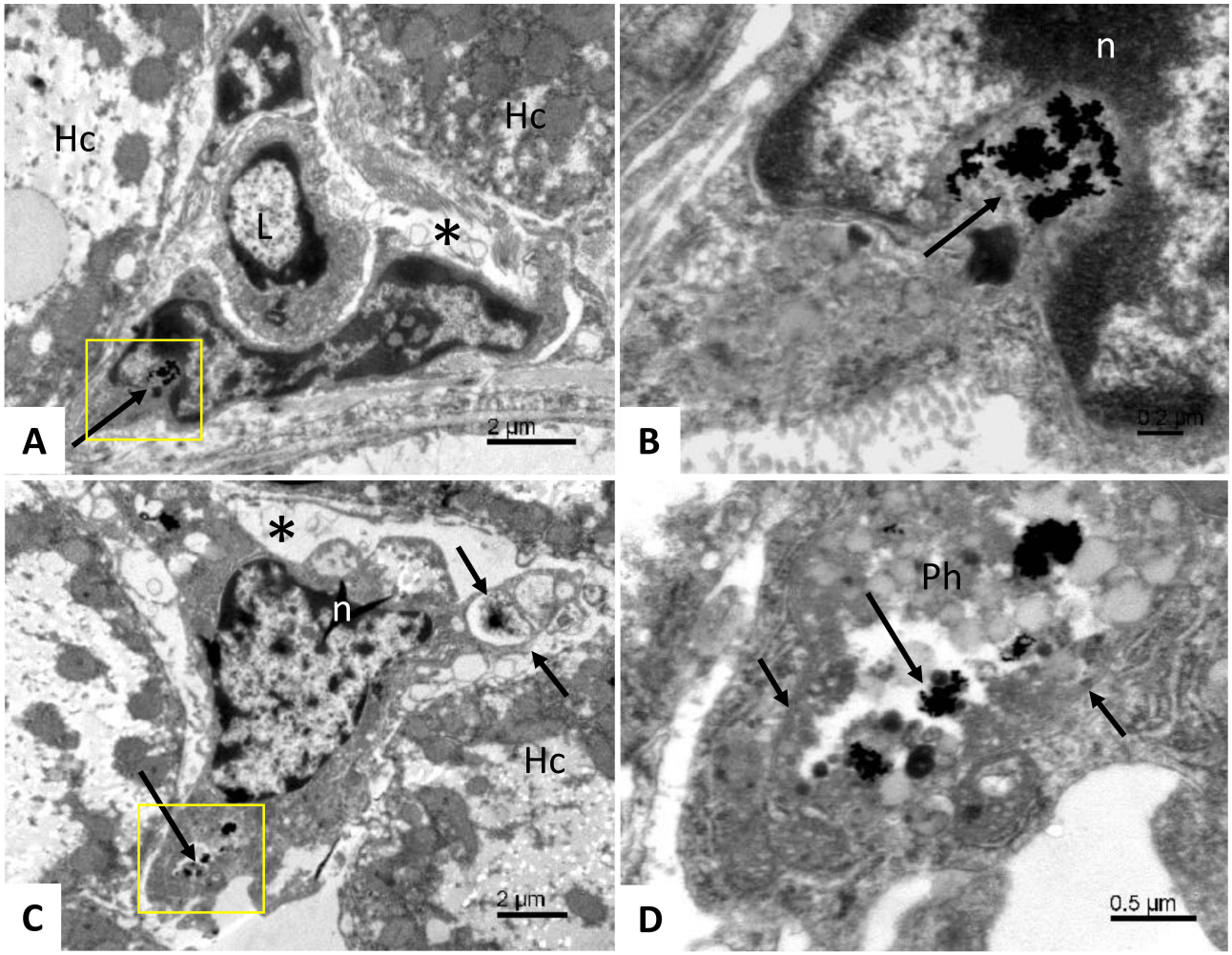

Figure 5 Accumulation of BSA-coated gold nanoparticles in the liver. Area of liver tissue cells showing hepatocytes (Hc); asterisk – a sinusoid in the lumen of which a lymphocyte is present (L); the lower part of the sinusoid is lined by an endothelial cell with a large cell nucleus; long arrow - clusters of gold nanoparticles located in the cytoplasm near the cell nucleus (**A**). Detail from figure (**A**) (yellow square); long arrow - clusters of gold nanoparticles in the endothelial cell cytoplasm; white n - cell nucleus (**B**). Phagocytic cell with gold nanoparticles (yellow square, long arrow) located in the sinusoid (asterisk); short arrows – phagocyte cytoplasmic protrusions; white n – cell nucleus of a phagocyte; Hc - liver cell (**C**). Detail from figure (**C**) (yellow square); long arrow - clusters of gold nanoparticles in a phagocytic cell accumulated in a large phagolysosome (Ph); short arrows – phagolysosome membrane (**D**).

Long-Term Exposure to BSA-AuNPs Increases the Inflammatory Response in the Kidneys Despite a Negligible Amount of Internalized Nanoparticles

The long-term exposure to BSA-AuNPs accumulated in the mouse body caused damage to the kidneys. Uptake of BSA-AuNPs in the kidneys was detected near threshold values, as indicated by ICP-MS (Figure 2A and C). Although BSA-AuNPs were almost undetectable in this organ, considerable structural changes in renal tissues were observed, which may affect kidney function. The weight of the kidneys in mice treated with BSA-AuNPs for 120 days did not differ from that in control animals (Figure 7A). ICP-MS measurement of the content of gold in the kidneys indicated the accumulation of BSA-AuNPs during the course of the experiment (Figure 7B), although the values measured represented a small fraction of the gold content in the liver even after adjusting for organ weight (Figure 7C). Higher levels of albumin were detected in the urine of mice with long-term BSA-AuNP exposure (Figure 7D), which is an indicator of damage to the filtration apparatus of the kidney. The cause of the glomerular leakage of albumin was investigated by histological examination of renal tissue. Periodic acid Schiff staining detected glomeruli with a higher amount of mesangium in the kidneys of mice treated with BSA-AuNPs for 120 days, which was further confirmed by staining for fibronectin (Figure 7E). Infiltration of F4/80 positive cells into renal tissues was also detected in mice exposed to BSA-AuNPs (Figure 7E). Examination of

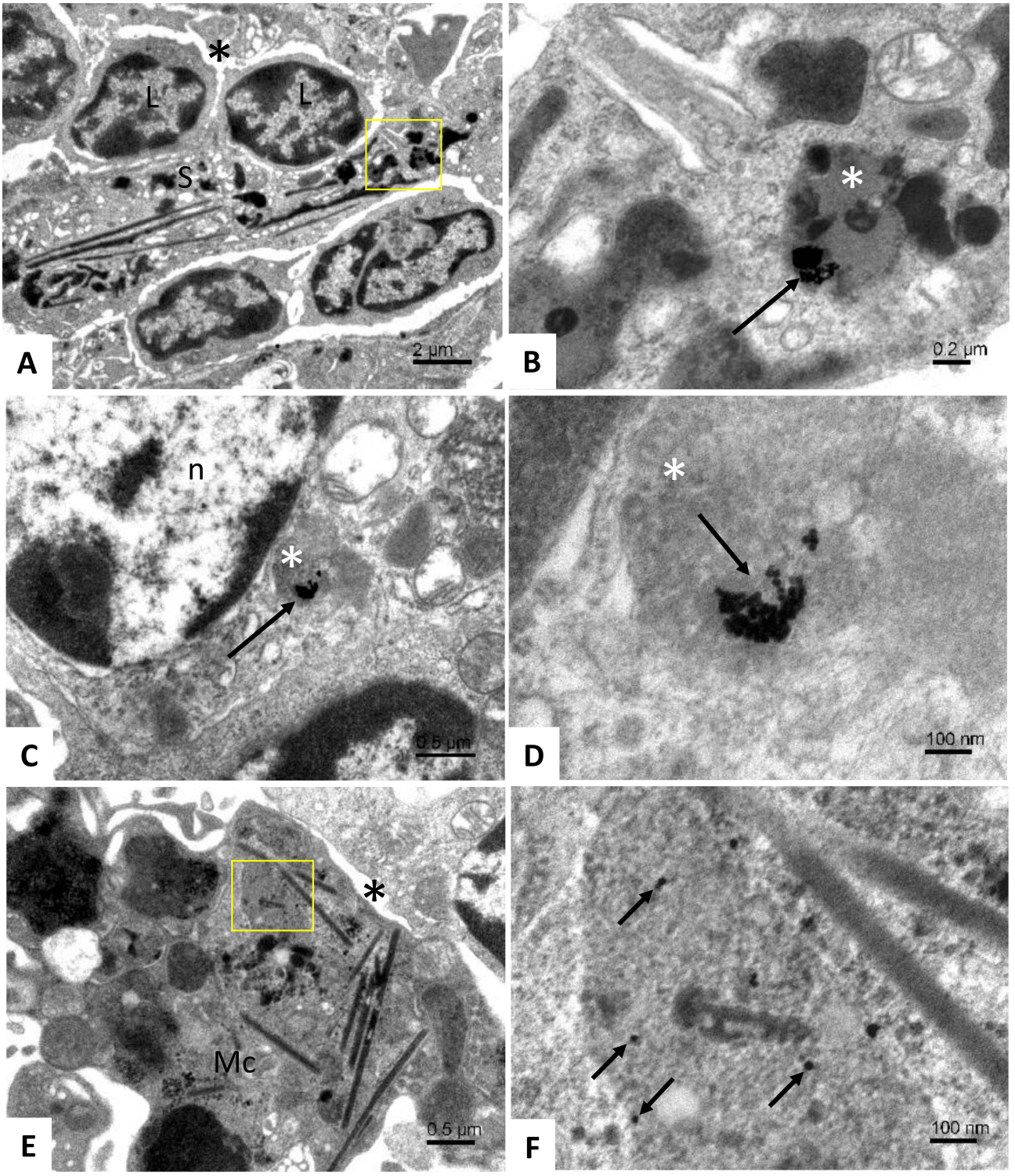

Figure 6 Accumulation of BSA-coated gold nanoparticles in the white pulp of spleen. Area of spleen tissue cells showing an supporting elongated cell (S) in the cytoplasm of which gold nanoparticles can be observed (yellow square); asterisk – a sinusoid; L –lymphocytes (**A**). Detail from figure A (yellow square); long arrow - clusters of gold nanoparticles located in the lysosome (white asterisk) (**B**). Area of endothelial cell; long arrow - gold nanoparticles found in the lysosome of the cell (white asterisk); n - cell nucleus (**C**). Detail from figure C; view of a cluster of gold nanoparticles (long arrow) located in a lysosome (white asterisk) (**D**) A macrophagic cell (Mc) in the space of the sinusoid (asterisk); scattered gold nanoparticles are found in the cytoplasm of the macrophage (yellow square) (**E**) Detail from figure E (yellow square); view of scattered gold particles (short arrows) localized in the macrophage lysosome (**F**).

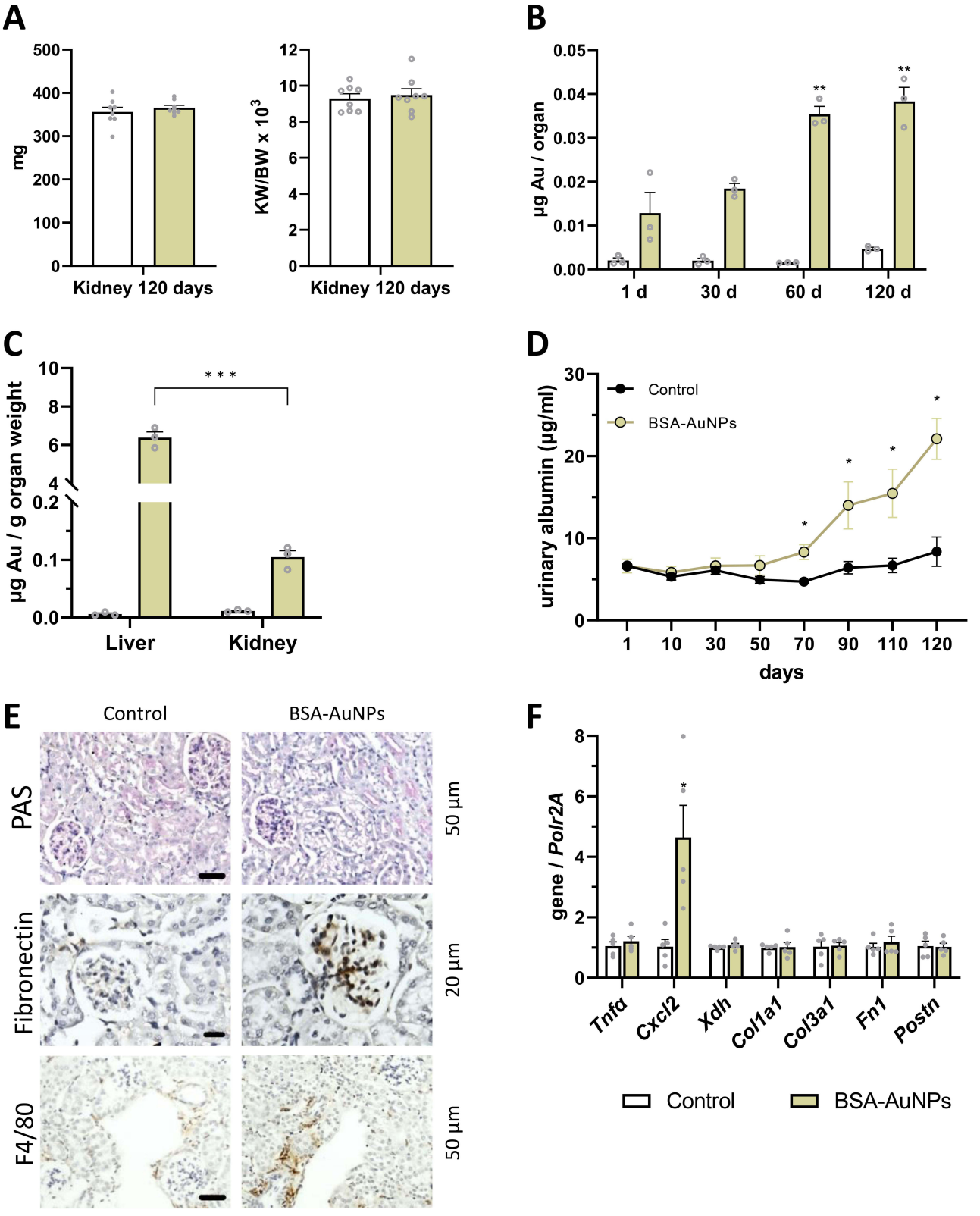

Figure 7 After 120 days from a single administration of nanoparticles, the kidney weight of the treated mice did not change compared to the control mice (**A**). Over time, there is an increased accumulation of nanoparticles in the kidneys (**B**), but this number of nanoparticles is small compared to the number of nanoparticles in the liver (**C**). Nevertheless, in mice that were treated with nanoparticles, after 70 days the level of albumin in the urine slightly increased compared to control mice (**D**). Higher amount of mesangium and fibronectin were identified in glomeruli. F4/80 positive cells were also detected in the renal tissue in BSA-AuNPs exposed mice (**E**). After 120 days, changes in the expression of Cxcl2 gene were observed in the kidney (**F**). Asterisks represent statistical differences between untreated and treated groups (**C, D** and **F**), or differences compared to 1 day (**B**). Data represent the mean ± SEM from three independent experiments (for qRT-PCR from five independent experiments and for level of albumin from eight independent experiments). Statistical significance among groups: $P < 0.05$ (*), $P < 0.01$ (**), and $P < 0.001$ (***). Magnification upper and lower panel 200x, bar 50 µm, middle panel 400x, bar 20 µm.

markers associated with inflammatory or fibrotic injury to renal tissues did not show increased expression of *Tnfα, Xdh, Col1a1, Col1a3, Fn1*, and *Postn*, whereas *Cxcl2* expression was increased (Figure 7F). The changes in the filtration apparatus caused by the presence of BSA-AuNPs were moderate rather than severe, which may explain these findings. However, due to the heterogeneity of kidneys, changes affecting small cell populations such as renal glomeruli can be masked by abundant populations such as renal tubules in the analysis of whole tissue lysates. *Cxcl2* synthesized by inflammatory cells at a site of inflammation indicates the presence of F4/80 positive cells in renal tissues and their activity after the long-term persistence of BSA-AuNPs in the mouse body. Tubular damage resulting from the long-term accumulation of BSA-AuNPs in the mouse was detected as well (Figure S4). These findings are consistent with the increase in urinary albumin levels in mice after long-term exposure to BSA-AuNPs despite a negligible amount of nanoparticles detected in renal tissues.

Discussion

Recent progress in nanomaterial research has facilitated the use of gold nanoparticles for medical applications. In line with this, comprehensive examination of the long-term biological safety of different AuNPs platforms assumed importance. Consistent with this aim, 120-day period was chosen to investigate the distribution and biological effects of BSA-AuNPs, in our study. Single intravenous administration of BSA-AuNPs into C57BL/6 mice was followed by monitoring of their biological effects in three vital organs: liver, spleen, and kidneys. The distribution of BSA-AuNPs in other organs was not investigated. Therefore, approximately half of the injected dose of BSA-AuNPs was either accumulated in the non-tested organs or may have been excreted from the mouse body, at least in part. Nevertheless, the elimination of BSA-AuNPs from the organs analyzed during a 4-month period suggested inefficient clearance of gold nanoparticles from the tissues. Measurements of BSA-AuNPs organ deposition over this period indicated that mechanisms underlying organ distribution, accumulation and elimination of BSA-AuNPs likely involved also secondary re-distribution and re-accumulation suggesting a very complex response of the organism to AuNPs presence. Increased accumulation of nanoparticles in the liver and kidneys was reported previously for QD705 Cd-core quantum dots for period of 28 days.[21] Despite extensive research in area of gold nanomaterials, such long-term observations are rare for AuNPs. The reason for the missing data may lie in the design of studies aimed preferably at the periods much shorter than 30 days.[22–25] Our results showed that in the first 30 days, the amount of BSA-AuNPs remained stable in the liver and increased in the spleen. The amount of gold detected in the kidneys was too small compared to liver and spleen, still, there was an increase detectable in the renal BSA-AuNPs accumulation up to 30 days. More dramatic changes, however, occurred in the next 90 days of investigation. Between days 30 and 120, the amount of BSA-AuNPs in the liver decreased by approximately 20% and increased in the spleen by approximately 38%. For the kidneys, a 100% increase has been detected. The slow release of BSA-AuNPs from the liver and subsequent intensive internalization of nanoparticles by the spleen may partially explain the inefficient elimination of BSA-AuNPs from the tissues and potentially from the mouse body, as such re-distribution and re-accumulation may have occurred in the other organs, too. After 4 months of exposure to a single dose of BSA-AuNPs, the nanoparticles were not cleared from any of the three organs – liver, spleen, and kidneys. Four months in the mouse life is equivalent to approximately 34 years in human life.[26] This might indicate that AuNPs may potentially remain in the human body for decades, and whether they would ever be completely eliminated from the target organs remains elusive for now. This surely should not prevent the clinical use of AuNPs. It only implies that their potential hazard to human health concerning the long-term toxicity should be thoroughly monitored.

Number of studies have suggested several therapeutic applications of AuNPs based on their properties such as minimal toxicity and biocompatibility.[27–29] Although gold nanoparticles are considered among the safest metallic nanoparticles,[30,31] their toxicity is a topic of considerable debate.[11,32,33] Several studies investigating AuNPs coated with other materials than BSA, reported adverse effects during shorter experimental periods than we used in our study.[15,34,35] The literature about investigation of toxicologic effects of AuNPs for potential biomedical applications indicated 0.137–2.200 mg/kg dose interval used for intravenous application.[17] Considering real future extrapolation into the clinics, we used concentration 1 mg/kg for our investigation of the long-term biological effects. This is in line with the recent data showing that 1 mg/kg AuNPs might be around the real therapeutical dose.[25,36,37] BSA-AuNPs are

considered a safe platform among various AuNPs types, nevertheless, their biocompatibility still needs to be carefully assessed. In one of the recent publications, five different doses of AuNPs coated with BSA ranging from 1.16 mg/kg to 5.84 mg/kg were tested for 8 consecutive days after intravenous injections in mice. No obvious changes in organ cell morphology were observed except for mitochondrial degradation in the liver in the highest dose group.[14] Mitochondria degradation alone may seem to indicate only a weak impact of AuNPs on the liver tissue. However, mitochondria are the key signaling organelles of the innate immune system and their degradation may be evidence of a strong immune response and breakdown of the metabolism control in the liver cells. The accumulation of damaged mitochondria is also associated with liver disease.[38,39] In this context, the dose of 1 mg/kg body weight used in our study was similar to the lowest dose in the aforementioned publication. In agreement with that study, yet applying a single dose of BSA-AuNPs but 10-fold longer follow-up period, we did not observe substantial changes in the organ function, but rather mild though significant changes in the structure of the tissues. Majority of changes were detected at the molecular level like increases in mRNA for *Tnf-α, Cxcl2*, and *Fn1*, indicating that exposure of the mouse organism to BSA-AuNPs for 120 days might activate expression of genes associated with inflammatory processes and fibrogenesis in liver, spleen, and kidneys. Interestingly, these changes were not detectable until 60 days of exposure, suggesting the late onset of the effects after the BSA-AuNPs administration, not reaching substantial structural alterations of the tissues at this point. These results are consistent with two reports presenting no obvious changes of the liver and spleen several months after a single injection of gold nanoparticles.[40,41] However, as evidence was based on hematoxylin-eosin staining and no immunohistology or other specific qualitative or quantitative analyses have been performed, no deeper comparison between the two studies and our study can be drawn. Taken this into consideration, this is the first study reporting nano-bio interactions of BSA-AuNPs in the tissues for a period of 120 days in the mouse. Moreover, immunohistochemical analyses brought important added value to the hematoxylin-eosin staining in our investigation. Increased fibronectin in vessel areas of liver with infiltrates of mononuclear cells (majority F4/80 positive) were consistent with the upregulation of the proinflammatory mediators *Tnf-α* and *Cxcl2* in the liver tissue. NASH parameters revealed the ability of BSA-AuNPs to cause liver cell damage. This was further confirmed by TEM displaying increased internalization of BSA-AuNPs in phagocytic cells in the liver after the long-term exposure. Potential involvement of immune cells such as phagocytes in the transport of BSA-AuNPs from the liver has already been discussed previously.[42] Interestingly, phagocytic cells that we analyzed in the spleen showed dispersed BSA-AuNPs in their vesicles compared to clusters of nanoparticles detected in the liver phagocytes. This would imply a higher degree of BSA-AuNPs degradation in the spleen and point at possible transport of BSA-AuNPs from the liver to the spleen. The transport of AuNPs by phagocytic cells, however, may not be limited to the spleen. Immune cells transporting the gold nanomaterial into the circulation may eventually travel to different organs (eg, kidneys) and so increase the accumulation of nanoparticles not only in organs with high but also with low primary distribution - as we have observed in the kidneys after the 120 days of exposure.

The primary biodistribution of AuNPs may vary according to nanoparticle size and coating. Previous study reported considerable amounts of PEG-coated AuNPs in renal tissue after 7 days with no detection of kidney injury.[35] We detected just the trace amounts of BSA-AuNPs in the kidneys during 120 days. Despite such low nanoparticle deposition, we identified fibrotic changes in renal glomeruli after this period. At present, we only can speculate whether this manifestation was related to the accumulated BSA-AuNPs or was it rather related to the role of the kidney in the blood filtration and filtered substances activated glomerular cells. Again, histological examination showed that increased glomerular fibronectin was related to F4/80-positive cells around vessels, which was further in line with increased *Cxcl2* mRNA in the renal tissue. Albumin detected in the urine confirmed the early damage to the renal filtration unit. The main cause for the development of albuminuria and subsequent glomerulosclerosis is considered the glomerular hyperfiltration.[43] Increased albuminuria detected in the urine of BSA-AuNPs exposed mice was directly associated with increased glomerular fibronectin, indicating that the cause for this initial stage of glomerulosclerosis might potentially involve glomerular hyperfiltration. Of note, glomerular deposits of fibronectin and the onset of albuminuria are signs of glomerular damage that, if left untreated, may progress to severe renal dysfunction.[44,45] Generally, albuminuria, serum creatinine and GFR are considered the major markers for the risk of kidney disease progression.[46] Although we have not estimated the serum creatinine and GFR and this aspect is a limitation of our study, increased renal fibronectin mRNA and fibronectin content in the glomeruli of BSA-AuNPs treated mice together with the urine albumin measurement

confirm the impairment of the renal function. A similar result was published in rats showing that mononuclear infiltration and inflammatory processes caused by exposure to repeated doses of AuNPs were responsible for the development of kidney fibrosis, whereas the intensity of the inflammatory response and enhanced accumulation of collagen correlated with the applied dose of AuNPs.[47] In light of previous studies reporting the negative side effects of gold therapy on kidney function, our results of BSA-AuNPs-mediated renal damage are not surprising. Patients with rheumatoid arthritis undergoing chrysotherapy showed signs of nephrotoxicity related to exposure to gold such as glomerulonephritis and proteinuria.[48–50] Toxicity related to gold ions was shown to be involved in the pathogenesis of tubular lesions, while immune complex glomerulonephritis was shown to be related to immunologically mediated drug (gold) toxicity.[50] Interestingly, the gold content was detected in the tissues for up to 23 years after the therapy was stopped.[51] Therefore, it is conceivable, that recent gold nanomaterials may exert similar effects given their long-term organ accumulation due to extremely slow elimination from the body.

Conclusion

In this work, the consequences of the long-term exposure to AuNPs on the structure and function of three vital organs – liver, spleen, and kidneys have been studied to help identify the key features of AuNPs accumulation in the tissues that might lead to their toxicity. The long-term accumulation of BSA-AuNPs in the liver and spleen did not affect the function of the two organs. However, detected changes in the structure of these organs including increased infiltration of macrophages and increased fibronectin level suggested toxic response associated with the chronic exposure to AuNPs. Whether such changes are transient and would resolve over the time or they represent an initial stage of a progressive inflammatory process need to be confirmed further. Increased fibronectin in renal glomeruli associated with albuminuria, despite negligible BSA-AuNPs accumulation in the kidneys, underline the complex response of the organism to the long-term nanoparticle deposition, which should be considered by AuNPs toxicological profiling. It would be interesting to find out whether such early signs of a kidney injury could be avoided through the use of pharmaceuticals. In summary, our results show that despite generally declared biocompatibility, AuNPs may contribute to adverse effects in the organs owing their slow elimination and subsequent long-term deposition in the tissues. Understanding these mechanisms and their contribution to the long-term toxicity of AuNPs may help by the development of safe-by-design strategies assessing AuNPs for future therapeutical applications.

Abbreviations

ALT, alanine transaminase; AuNPs, gold nanoparticles; BSA, bovine serum albumin; BSA-AuNPs, bovine serum albumin coated gold nanoparticles; Col1a1, collagen type I; Col1a3, collagen type III; Cxcl2, chemokine ligand 2; DLS, dynamic light scattering; ELISA, enzyme linked immunosorbent assay; FE-SEM, Field Emission Scanning Electron Microscopy; Fn1, fibronectin; HE, haematoxylin eosin staining; ICP-MS, Inductively coupled plasma mass spectroscopy; NASH, non-alcoholic steatohepatitis; PAS, periodic acid-Schiff reaction; PMSF, Phenylmethylsulfonyl fluoride; Polr2a, RNA polymerase II subunit A; Postn, periostin; RT, room temperature; SPF, Specific Pathogen-Free; TEM, transmission electron microscopy; Tnfα, tumor necrosis factor alpha; Xdh, Xanthine Dehydrogenase.

Acknowledgments

The authors thank the Slovak Cancer Research Foundation, for OLYMPUS BX46 microscope and L. Novota (Institute of Experimental Endocrinology, Biomedical Research Center, SAS) for expert assistance with the electron microscopy. This study was performed during the implementation of the project Building-up Centre for advanced materials application of the Slovak Academy of Sciences, ITMS project code 313021T081 supported by Research & Innovation Operational Programme funded by ERDF.

Funding

This work was supported by the Slovak Research and Development Agency under Contract No. APVV-16-0579 and APVV-20-0494, and by VEGA grant no. 2/0116/22.

Disclosure

The authors report no conflicts of interest in this work.

References

1. Dykman LA, Khlebtsov NG. Gold nanoparticles in biology and medicine: recent advances and prospects. *Acta Naturae*. 2011;3(2):34–55. doi:10.32607/20758251-2011-3-2-34-55
2. Li X, Zhang Y, Liu GK, et al. Recent progress in the applications of gold-based nanoparticles towards tumor-targeted imaging and therapy. *RSC Adv*. 2022;12(13):7635–7651. doi:10.1039/d2ra00566b
3. Hu X, Zhang Y, Ding T, et al. Multifunctional gold nanoparticles: a novel nanomaterial for various medical applications and biological activities. *Front Bioeng Biotechnol*. 2020;8. doi:10.3389/fbioe.2020.00990
4. Dreaden EC, Alkilany AM, Huang X, et al. The golden age: gold nanoparticles for biomedicine. *Chem Soc Rev*. 2012;41:2740–2779. doi:10.1039/c1cs15237h
5. Alric C, Taleb J, Le Duc G, et al. Gadolinium chelate coated gold nanoparticles as contrast agents for both X-ray computed tomography and magnetic resonance imaging. *J Am Chem Soc*. 2008;130(18):5908–5915. doi:10.1021/ja078176p
6. Sibuyi NRS, Moabelo KL, Fadaka AO, et al. Multifunctional gold nanoparticles for improved diagnostic and therapeutic applications: a review. *Nanoscale Res Lett*. 2021;16(1). doi:10.1186/s11671-021-03632-w
7. Arnida, Janát-Amsbury MM, Ray A, Peterson CM, Ghandehari H, Ghandehari H. Geometry and surface characteristics of gold nanoparticles influence their biodistribution and uptake by macrophages. *Eur J Pharm Biopharm*. 2011;77(3):417–423. doi:10.1016/j.ejpb.2010.11.010
8. Lasagna-Reeves C, Gonzalez-Romero D, Barria MA, et al. Bioaccumulation and toxicity of gold nanoparticles after repeated administration in mice. *Biochem Biophys Res Commun*. 2010;393(4):649–655. doi:10.1016/j.bbrc.2010.02.046
9. Pan Y, Leifert A, Ruau D, et al. Gold nanoparticles of diameter 1.4 nm trigger necrosis by oxidative stress and mitochondrial damage. *Small*. 2009;5(18):2067–2076. doi:10.1002/smll.200900466
10. Goodman CM, McCusker CD, Yilmaz T, et al. Toxicity of gold nanoparticles functionalized with cationic and anionic side chains. *Bioconjugate Chem*. 2004;15(4):897–900. doi:10.1021/bc049951i
11. Sani A, Cao C, Cui D. Toxicity of gold nanoparticles (AuNPs): a review. *Biochem Biophys Rep*. 2021;26:100991. doi:10.1021/bc049951i
12. Fraga S, Brandão A, Soares ME, et al. Short- and long-term distribution and toxicity of gold nanoparticles in the rat after a single-dose intravenous administration. *Nanomedicine*. 2014;10(8):1757–1766. doi:10.1016/j.nano.2014.06.005
13. Abu-Dief AM, Salaheldeen M, El-Dabea T. Recent advances in development of gold nanoparticles for drug delivery systems. *J Mod Nanotechnol*. 2021;1(1). doi:10.53964/jmn.2021001
14. Nghiem THL, Nguyen TT, Fort E, et al. Capping and in vivo toxicity studies of gold nanoparticles. *Adv Nat Sci*. 2012;3(1):015002.
15. Brewer SH, Glomm WR, Johnson MC, et al. Probing BSA binding to citrate-coated gold nanoparticles and surfaces. *Langmuir*. 2005;21(20):9303–9307. doi:10.1021/la050588t
16. Zhang XD, Wu D, Shen X, et al. Size-dependent in vivo toxicity of PEG-coated gold nanoparticles. *Int j Nanomed*. 2011;6:2071–2081. doi:10.2147/IJN.S21657
17. Zhang XD, Wu HY, Wu D, et al. Toxicologic effects of gold nanoparticles in vivo by different administration routes. *Int j Nanomed*. 2010;5:771–781. doi:10.2147/IJN.S8428
18. Kimling J, Maier M, Okenve B, et al. Turkevich method for gold nanoparticle synthesis revisited. *J Phys Chem B*. 2006;110(32):15700–15707. doi:10.1021/jp061667w
19. Nemethova V, Buliakova B, Mazancova P, et al. Intracellular uptake of magnetite nanoparticles: a focus on physico-chemical characterization and interpretation of in vitro data. *Mater Sci Eng*. 2017;70:161–168. doi:10.1016/j.msec.2016.08.064
20. Wu Y, Cao Y, Xu K, et al. Dynamically remodeled hepatic extracellular matrix predicts prognosis of early-stage cirrhosis. *Cell Death Dis*. 2021;12(2):163. doi:10.1038/s41419-021-03443-y
21. Yang RSH, Chang LW, Wu JP, et al. Persistent tissue kinetics and redistribution of nanoparticles, quantum Dot 705, in Mice: ICP-MS quantitative assessment. *Environ Health Perspect*. 2007;115(9):1339–1343. doi:10.1289/ehp.10290
22. Lopez-Chaves C, Soto-Alvaredo J, Montes-Bayon M, et al. Gold nanoparticles: distribution, bioaccumulation and toxicity. In vitro and in vivo studies. *Nanomedicine*. 2018;14(1):1–12. doi:10.1016/j.nano.2017.08.011
23. de Jong WH, Hagens WI, Krystek P, et al. Particle size-dependent organ distribution of gold nanoparticles after intravenous administration. *Biomaterials*. 2008;29(12):1912–1919. doi:10.1016/j.biomaterials.2007.12.037
24. Aravinthan A, Kamala-Kannan S, Govarthanan M, et al. Accumulation of biosynthesized gold nanoparticles and its impact on various organs of Sprague Dawley rats: a systematic study. *Toxicol Res*. 2016;5(6):1530–1538. doi:10.1039/c6tx00202a
25. Kozics K, Sramkova M, Kopecka K, et al. Pharmacokinetics, Biodistribution, and Biosafety of PEGylated Gold Nanoparticles In Vivo. *Nanomaterials*. 2021;11(7):1702. doi:10.3390/nano11071702
26. Dutta S, Sengupta P. Men and mice: relating their ages. *Life Sci*. 2016;152:244–248. doi:10.1016/j.lfs.2015.10.025
27. Vines JB, Yoon JH, Ryu NE, et al. Gold nanoparticles for photothermal cancer therapy. *Front Chem*. 2019;7:167. doi:10.3389/fchem.2019.00167
28. Jain S, Hirst DG, O'Sullivan JM. Gold nanoparticles as novel agents for cancer therapy. *Br J Radiol*. 2012;85(1010):101–113. doi:10.1259/bjr/59448833
29. Yang Y, Zheng X, Chen L, et al. Multifunctional gold nanoparticles in cancer diagnosis and treatment. *Int j Nanomed*. 2022;17:2041–2067. doi:10.2147/IJN.S355142
30. Downs TR, Crosby ME, Hu T, et al. Silica nanoparticles administered at the maximum tolerated dose induce genotoxic effects through an inflammatory reaction while gold nanoparticles do not. *Mutat Res*. 2012;745(1–2):38–50. doi:10.1016/j.mrgentox.2012.03.012
31. Schulz M, Ma-Hock L, Brill S, et al. Investigation on the genotoxicity of different sizes of gold nanoparticles administered to the lungs of rats. *Mutat Res*. 2012;745(1–2):51–57. doi:10.1016/j.mrgentox.2011.11.016
32. Javed I, Hussain SZ, Shahzad A, et al. Lecithin-gold hybrid nanocarriers as efficient and pH selective vehicles for oral delivery of diacerein-In-vitro and in-vivo study. *Colloids Surf B*. 2016;141:1–9. doi:10.1016/j.colsurfb.2016.01.022

33. Paino IMM, Marangoni VS, de Oliveira R de CS, et al. Cyto and genotoxicity of gold nanoparticles in human hepatocellular carcinoma and peripheral blood mononuclear cells. *Toxicol Lett*. 2012;215(2):119–125. doi:10.1016/j.toxlet.2012.09.025
34. Liu H, Liu T, Wang H, et al. Impact of PEGylation on the biological effects and light heat conversion efficiency of gold nanoshells on silica nanorattles. *Biomaterials*. 2013;34(28):6967–6975. doi:10.1016/j.biomaterials.2013.05.059
35. Cho WS, Cho M, Jeong J, et al. Acute toxicity and pharmacokinetics of 13 nm-sized PEG-coated gold nanoparticles. *Toxicol Appl Pharmacol*. 2009;236(1):16–24. doi:10.1016/j.taap.2008.12.023
36. Brzoska K, Szczygiel M, Drzał A, et al. Transient vasodilation in mouse 4T1 tumors after intragastric and intravenous administration of gold nanoparticles. *Int J Mol Sci*. 2021;22(5):2361. doi:10.3390/ijms22052361
37. Komatsu T, Nakamura K, Okumura Y, Konishi K. Optimal method of gold nanoparticle administration in melanoma-bearing mice. *Exp Ther Med*. 2018;15(3):2994–2999. doi:10.3892/etm.2018.5746
38. Degli Esposti D, Hamelin J, Bosselut N, et al. Mitochondrial roles and cytoprotection in chronic liver injury. *Biochem Res Int*. 2012;387626. doi:10.1155/2012/387626
39. Zhang IW, López-Vicario C, Duran-Güell M, et al. Mitochondrial dysfunction in advanced liver disease: emerging concepts. *Front Mol Biosci*. 2021;8:772174. doi:10.3389/fmolb.2021.772174
40. Ali MRK, Rahman MA, Wu Y, et al. Efficacy, long-term toxicity, and mechanistic studies of gold nanorods photothermal therapy of cancer in xenograft mice. *Proc Natl Acad Sci USA*. 2017;114:3110–3118. doi:10.1073/pnas.1619302114
41. Cho WS, Cho M, Jeong J, et al. Size-dependent tissue kinetics of PEG-coated gold nanoparticles. *Toxicol Appl Pharmacol*. 2010;245(1):116–123. doi:10.1016/j.taap.2010.02.013
42. Poon W, Zhang YN, Ouyang B, et al. Elimination Pathways of Nanoparticles. *ACS Nano*. 2019;13(5):5785–5798. doi:10.1021/acsnano.9b01383
43. Melsom T, Stefansson V, Schei J, et al. Association of increasing GFR with change in albuminuria in the general population. *Clin J Am Soc Nephrol*. 2016;11(12):2186–2194. doi:10.2215/CJN.04940516
44. Babelova A, Avaniadi D, Jung O, et al. Role of Nox4 in murine models of kidney disease. *Free Radic Biol Med*. 2012;53(4):842–853. doi:10.1016/j.freeradbiomed.2012.06.027
45. Bülow RD, Boor P. Extracellular matrix in kidney fibrosis: more than just a scaffold. *J Histochem Cytochem*. 2019;67(9):643–661. doi:10.1369/0022155419849388
46. Norris KC, Smoyer KE, Rolland C, et al. Albuminuria, serum creatinine, and estimated glomerular filtration rate as predictors of cardio-renal outcomes in patients with type 2 diabetes mellitus and kidney disease: a systematic literature review. *BMC Nephrol*. 2018;19(1):36. doi:10.1186/s12882-018-0821-9
47. Elwan WM, Ragab AMH, Ragab MH. Histological and immunohistochemical evaluation of the dose-dependent effect of gold nanoparticles on the renal cortex of adult female albino rat. *Egypt J Histol*. 2018;41(2):167–181. doi:10.21608/EJH.2018.13839
48. Hall CL, Tighe R. The effect of continuing penicillamine and gold treatment on the course of penicillamine and gold nephropathy. *Br J Rheumatol*. 1989;28(1):53–57. doi:10.1093/rheumatology/28.1.53
49. Robbins G, McIllmurray MB. Acute renal failure due to gold. *Postgrad Med J*. 1980;56(655):366–367. doi:10.1136/pgmj.56.655.366
50. Antonovych TT. Gold Nephropathy. *Ann Clin Lab Sci*. 1981;11(5):386–391.
51. Derot M, Kahn J, Mazalton A, et al. Fatal acute anuric nephritis after gold therapy, with associated chrysocyanosis. *Bulletins Et Memoires de la Societe Medicale Des Hopitaux de Paris*. 1954;70(7–8):234–239.